



# Micromechanical modeling of particle breakage of granular materials in the framework of thermomechanics

Chaomin Shen<sup>1</sup> · Sihong Liu<sup>1</sup> · Liujiang Wang<sup>1</sup> · Yishu Wang<sup>1</sup>

Received: 29 August 2017 / Accepted: 5 July 2018  
© Springer-Verlag GmbH Germany, part of Springer Nature 2018

## Abstract

The particle breakage of granular materials under compression is a phenomenon of great importance. In this paper, a micromechanically based model for the compression of crushable granular materials is developed in the framework of thermomechanics. Both the internal and dissipative energies in the model are derived using the micro–macro volume averaging approach to ensure that all parameters involved have concrete physical meanings. The particle breakage is quantified by the change of the maximum particle size, the size polydispersity and the fractal dimension of the gradation. Compared to other breakage models, there is a major difference that highlights the novelty of the proposed model: neither the ultimate particle size distribution, nor the evolution path of the gradation is predefined in the model. The initiation, evolution and the attenuation of the breakage can be determined by the maximum dissipation principle using thermomechanics and micromechanics. Finally, it is demonstrated that the proposed model can predict the stress dependence of the elastic bulk modulus, the size dependence of the yielding stress and the elastic–plastic–pseudoelastic phase transition of granular materials.

**Keywords** Granular material · Micromechanics · Particle breakage · Physically based model · Thermomechanics

## 1 Introduction

One of the today's great challenges in geomechanics is to understand the role of particle breakage in the mechanical behavior of crushable granular materials like sands and rockfills. Particle breakage may take place not only under high stress conditions, but also under low stress conditions for weak-grained crushable granular materials such as carbonate sands or decomposed granites. In geotechnical engineering practices, particle breakage gives rise to various problems, such as the piles creep in sand [32], the additional settlement of high rockfill dams [2] and the nonlinear strength envelope of rail ballast [17]. It is also of prime importance in the critical state constitutive theories [1, 16, 56]. For example, a key question in the mechanics of sands is what role particle breakage plays in the location of the critical state line in the plane of the void ratio against

the logarithm of mean effective stress [36]. For these reasons, particle breakage has increasingly interested many technological and theoretical fields of research.

A good starting point to investigate particle breakage of granular materials is often under the condition of compression. Extensive experiments indicate that the particle breakage of granular materials under compression is influenced by many factors, such as the magnitude of the applied stress [45, 47, 59], the particle strength [26, 30], the particle size [25, 31, 39, 41], the particle size distribution (PSD) [30, 31] and the initial compactness of the material [25, 58]. Consequently, the forms of the compression curve (i.e., the relationship between the void ratio and the effective stress) of granular materials may differ [42] and several models have been proposed to describe the compression curves [5, 47, 53]. In general, three phases have been generally identified in the compression curves: volume decrease at low stresses, more intense compression due to particle breakage under higher stresses and the pseudoelastic behavior at very high stresses [25].

Apart from laboratory tests, the discrete element method (DEM) is also an effective technique to study the particle

✉ Sihong Liu  
sihongliu@hhu.edu.cn

<sup>1</sup> College of Water Conservancy and Hydropower Engineering, Hohai University, Nanjing 210098, China

breakage. It has been proven to be one powerful tool in capturing the micromechanical behaviors of crushable granular materials [33, 34, 52]. Two methods are generally used to simulate particle breakage by DEM: bonding method and splitting method. The bonding method was pioneered by Robertson [48], who explored the procedure of modeling crushable numerical grains created by bonding elementary balls (also called agglomerates). Cheng et al. [11] verified the Weibull statistics of the crushing strength of the agglomerates and discussed the role of particle breakage in the plasticity of granular materials. Further study on the energy balances during particle breakage by Bolton et al. [8] indicated that a typical particle breakage process is accompanied with the change of three energies: internal energy (elastic energy), energy dissipation due to particle breakage and the energy dissipation associated with frictional sliding and rolling triggered by the creation of new degrees of freedom among the breaking fragments. DEM simulations using agglomerates are also capable of considering the influence of particle shape and variability [3, 8, 11, 13] of crushable materials. Despite the energetic insight provided, the bonding model is limited in the computational efficiency, especially for polydisperse granular materials. The splitting method for the DEM simulation of particle breakage, which involves modeling grains with single particles and replacing them with smaller fragments, has also been used in the literature to simulate multigenerational particle breakage and to enhance the computational efficiency [4, 6, 9, 12, 40, 54]. An important application of this approach is to observe the evolution of the PSD of crushable granular materials under sufficiently large stress (e.g., [6, 12]). However, the choice of the breakage criterion and the breakage configuration in the splitting method is still a matter of debate. In addition, the energy conservation is not guaranteed in this method. Recently, a variety of new techniques including the combined FDEM [35] and the random virtual crack DEM [62] have been adopted to study more sophisticated problems.

To bridge the laboratory results and the micromechanical behaviors observed in DEM simulations, two representative theories have been proposed. The elastic mechanics was proposed by McDowell and Bolton [7, 39, 41], who quantified the survival probability of particles under compression with a modified Weibull distribution. They further formulated a new work equation that includes the energy dissipation due to grain crushing to provide a physical insight into the hardening parameter in critical state soil models. Einav [19–21] developed the theory of breakage mechanics using thermomechanics, in which the internal energy was related to the change of the PSD. By assuming the existence of an ultimate PSD for crushable granular materials, he established an elastic–plastic–breakage model where the evolution of the void

ratio as well as the PSD against the loading stress was considered. Both the elastic mechanics and the breakage mechanics provided remarkable insights into the physics of compression of crushable granular materials. However, as some empirical results had to be adopted in these models, the underlying physics of the particle breakage are not totally unveiled.

In this context, the main purpose of this study is to reveal the physics of particle breakage during compression. Compared with the existing models, the emphasis in the present work is mainly placed on: (1) understanding the driving thermodynamic mechanisms that control the yielding stress and evolution path of the PSD of crushable granular materials; (2) developing a model that predicts, rather than depicts the influence of particle breakage. For the sake of simplicity, the investigation is limited to the isotropic compression of frictionless spherical granular materials. An elastic–breakage model for the compression of granular materials is derived on micromechanics and the fundamental laws of thermomechanics. The capacity of the model is evaluated in comparison with experimental data and DEM simulations in the literature.

## 2 Outline of the thermomechanical modeling scheme

The general thermodynamics statement of a rate-independent mechanical procedure can be expressed as [19]

$$\dot{W} = \dot{u} + \dot{\Phi}, \quad \dot{\Phi} \geq 0 \quad (1)$$

where  $W$  is the work input per unit volume into the mechanical system;  $u$  and  $\Phi$  are the internal energy density and the dissipative energy density, respectively. The dot symbol over the variables denotes the time differential  $\partial/\partial t$ . For spherical frictionless granular systems under the isotropic compression, the general forms of  $u$  and  $\dot{\Phi}$  are defined as

$$u = u(\sigma_m, \Gamma), \quad \dot{\Phi} = \dot{\Phi}(\Gamma, \dot{\Gamma}) \quad (2)$$

where  $\sigma_m$  is the hydrostatic stress;  $\Gamma$  is designated as a generalized indicator of particle breakage and its form will be specified later. In general, particle breakage results in the rearrangement of particles, which may be accompanied with frictional dissipation. However, as Einav [19] pointed out, the plastic dissipation during the compression of crushable granular materials is secondary to the dissipation owing to breakage. Therefore, developing models that account for the breakage, without considering plastic straining, can be a good starting point before proceeding a full elastic–plastic–breakage analysis. Hence, this study

only focuses on the elastic-breakage process, which means  $\dot{\varepsilon}_v = \dot{\varepsilon}_v^e$ . As a result, the power input  $\dot{W}$  can be rewritten as:

$$\dot{W} = \sigma_m \dot{\varepsilon}_v = \sigma_m \dot{\sigma}_m / K_B^e \quad (3)$$

where  $\varepsilon_v$  is the volumetric strain and  $K_B^e$  is the elastic bulk modulus.

Substituting Eqs. (3) and (2) into (1) yields

$$\left( \sigma_m / K_B^e - \frac{\partial u}{\partial \sigma_m} \right) \dot{\sigma}_m = \frac{\partial u}{\partial \Gamma} \dot{\Gamma} + \dot{\Phi} \quad (4)$$

For a reversible thermomechanical process, i.e., a process without particle breakage, Eq. (4) leads to

$$\sigma_m / K_B^e - \frac{\partial u}{\partial \sigma_m} = 0 \quad (5)$$

As Eq. (4) also holds for the particle breakage process, by comparing Eq. (4) with Eq. (5), we can also obtain

$$\frac{\partial u}{\partial \Gamma} \dot{\Gamma} + \dot{\Phi} = 0 \quad (6)$$

The second law of thermodynamics requires that the dissipation  $\dot{\Phi}$  should be nonnegative. Therefore, it is obtained from Eq. (6) that  $\frac{\partial u}{\partial \Gamma} \dot{\Gamma} \leq 0$ , which implies that the particle breakage always tends to reduce the internal energy in the granular system. It is noted that the second law of thermodynamics requires only the non-negativity of the dissipation, which is obviously insufficient to determine the evolution path of energy densities. Thus, more strict conditions are required to determine the evolution of particle breakage.

In order to establish a model for the compression of crushable granular materials in the thermomechanical framework, one should address the following three questions: (1) how to determine the internal and dissipative energy densities? (2) how to specify the generalized indicator of particle breakage  $\Gamma$ ? (3) how to determine the evolution of the particle breakage? In what follows, these three questions will be answered successively: the energy densities are formulated using micromechanics in Sect. 3; the particle breakage indicator is proposed in Sect. 4; and the evolution law of the particle breakage is derived and a complete elastic-breakage model is established in Sect. 5.

### 3 Micro–macro formulation of energy densities

Regarding a possible method to determine the energy densities of crushable granular materials under isotropic compression, the micromechanical approach is potentially attractive because the micromechanics is capable of capturing the mechanism at the microscopic (particulate) scale

and homogenize it to the macroscopic scale. In this section, the internal and the dissipative energy densities at the particulate scale are firstly formulated in terms of its contact information in Sect. 3.1. Then, the particulate results in the total volume are averaged to the macroscopic scale in Sect. 3.2.

#### 3.1 Particulate scale

First of all, it is defined that the gradation of the granular material is described by a particle number distribution function  $p(r)$ , with  $\int_{r_{\min}}^{r_{\max}} p(r) dr = 1$ . The number of particles with radii ranging from  $r$  to  $r + dr$  is thus  $Np(r)dr$ , where  $N$  is the total particle number in the granular system.

##### 3.1.1 Internal energy density

In the case of one single spherical particle located within a granular media, it has been proven [29] that the microscopic stress can be expressed in terms of the contact forces  $f_i^c$  and their corresponding branch vectors  $l_j^c$ , given by

$$\sigma_{ij}^p = \frac{1}{V_p} \sum_{c \in V_p} f_i^c l_j^c \quad (7)$$

where the superscript  $c$  denotes the contacts and  $V_p$  is the volume of the particle. For a spherical particle, we have  $V_p = 4/3\pi r^3$  and the norm of the branch vector is  $|l_j^c| = r$ .

When the particle is compressed under a hydrostatic pressure, the mean stress of the particle, denoted as  $\sigma_m^p$ , is calculated from Eq. (7) as

$$\sigma_m^p = \frac{1}{3} \sigma_{ii}^p = \frac{1}{4\pi r^3} \sum_{c \in V_p} f_i^c l_i^c \quad (8)$$

For a frictionless granular system, the directions of the contact forces coincide with their corresponding branch vectors. Thus, Eq. (8) can be simplified as

$$\sigma_m^p = \frac{f(r)C(r)}{4\pi r^2} \quad (9)$$

where  $r$  is the radius of the spherical particle,  $f$  is the average of the magnitudes of the contact forces exerted on the particle, and  $C$  is the coordination number. Here, both of them are regarded as functions of the particle radius.

For two frictionless elastic spheres of radius  $r$  and  $r'$  pressed together under a load  $f$ , Hertz [27] established the force–displacement relation of the contact between them, expressed as

$$\Delta_t^3 = \Omega^3 f^2 \left( \frac{1}{r} + \frac{1}{r'} \right) \quad (10)$$

where  $\Delta_t$  is the total displacement that the two spheres approach each other.  $\Omega$  is a material parameter given by

$$\Omega^3 = \frac{9}{4} \left( \frac{1 - \nu^2}{\pi E} \right) \quad (11)$$

Equation (10) can be divided into two additive terms that are associated with the two contacting spheres, respectively. For the sphere with the radius  $r$ , its contribution to the total displacement is

$$\Delta = \Omega r^{-1/3} f^{2/3} \quad (12)$$

By adopting Eq. (12), the elastic energy stored within the particle with the radius  $r$  for one single contact can be calculated

$$E_c = \int_0^{\Delta} f(\Delta) d\Delta = \frac{2}{5} \Omega r^{-1/3} f^{5/3} \quad (13)$$

Consequently, the total elastic energy density stored within the particle can be obtained via summation of Eq. (13)

$$u^p = \frac{1}{V_p} \sum_{c \in V_p} E_c \quad (14)$$

As the average contact force and the coordination number of the particle have been regarded as functions of the particle radius, the total elastic energy density stored within the particle can be rewritten by combining Eqs. (13) and (14)

$$u^p(r) = \frac{2}{5V_p} \Omega r^{-1/3} [f(r)]^{5/3} C(r). \quad (15)$$

The coordination number  $C(r)$  in Eq. (15) for a particle with radius  $r$  is related to the sizes of its surrounding particles in the granular system. It is estimated in this study by mapping the neighboring particles onto the surface of the reference particle so that the “shaded area” is considered occupied. Given that the surface area of a regularly shaped particle is calculable, the maximum coordination number can be estimated by calculating the number of “occupations” available. This idea was first introduced by Ouchiyama and Tanaka [46] and was verified in the study on the trace of the fabric tensor in granular systems with narrow-size distributions in [37].

In this study, we extend this idea to a polydisperse granular system where the surrounding particles are of different sizes (see Fig. 1).

$R$  is the radius of a particle that surrounds the reference particle with radius  $r$ .  $S(r, R)$  denotes the area of the surface “shaded” by the surrounding particle, which can be calculated as

$$S(r, R) = 2\pi r^2 \left( 1 - \sqrt{\frac{2Rr + r^2}{(r + R)^2}} \right) \quad (16)$$

The radii  $R$  of the particles surrounding the reference particle should satisfy the same distribution as the PSD of

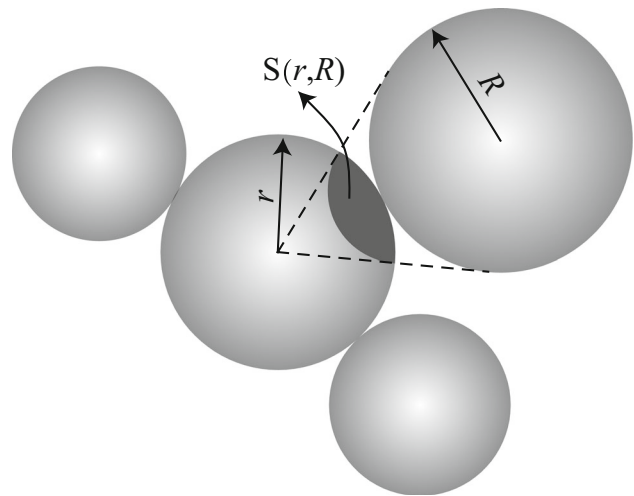


**Fig. 1** Schematic representation of a particle with radius  $r$  in contact with particles of different radii denoted by  $R$

the granular system. In this case, the mathematical expectation for one “shaded” area  $S(r)$  is

$$S(r) = 2\pi r^2 \int_{r_{\min}}^{r_{\max}} \left( 1 - \sqrt{\frac{2Rr + r^2}{(r + R)^2}} \right) p(R) dR \quad (17)$$

Taking into account the total surface area of the reference particle, one can obtain its coordination number

$$C(r) = \frac{4\pi r^2}{c_s S(r)} = \frac{2}{c_s \int_{r_{\min}}^{r_{\max}} \left( 1 - \sqrt{\frac{2Rr + r^2}{(r + R)^2}} \right) p(R) dR} \quad (18)$$

where  $c_s$  was defined as the linear capacity that describes the total fraction of the “shaded” surface [51]. The study in [51] suggested that  $c_s$  depends on the polydispersity of the granular system: it can be regarded as a constant in narrowly distributed granular systems, while it varies with the reference particle size in highly polydisperse granular systems. For the sake of simplicity, the variation of the linear capacity in highly polydisperse granular systems is not considered in this study.

By now, the stress and the internal energy density of one single particle in a granular system are related to the properties of its contacts via Eqs. (9) and (15), in which the coordination number  $C(r)$  is estimated by Eq. (18), but the contact force  $f(r)$  has not yet been determined and will be discussed later.

### 3.1.2 Dissipative energy density

At the microscopic level, the dissipative mechanism of granular materials under external compression may be interpreted as the result of the breakage of the particles and the relative frictional sliding or spin among particles [19].

As this study focuses on frictionless spherical particles, the dissipation due to the frictional sliding or spin is ignored.

The energy dissipation due to the particle breakage in a granular system is quantified by introducing the concept of strain energy release rate  $G_f$  in fracture mechanics [23]

$$\dot{\Phi}^p = G_f \dot{S}^p \quad (19)$$

where  $\Phi^p$  denotes the dissipative energy for a single particle;  $S^p$  is the surface area per unit volume and equals  $3/r$  for a spherical particle.

Equation (19) implies that the dissipative energy due to the particle breakage is proportional to the creation of the surface area. Similar concept that relates the breakage dissipation to the creation of the surface area was adopted to model the particle breakage in [41]. This hypothesis can also be supported by the results of triaxial compression tests on decomposed granite soil by Miura and Ohara [44].

### 3.2 Volume averaging

The purpose of this subsection is to determine both the internal and the dissipative energy densities of a granular system, so that they can be related to the microscopic quantities.

The homogenization approach chosen in this study is to take the averages of the microscopic quantities weighted by the volume of each particle, which can be expressed as

$$\langle X \rangle = \frac{1}{V} \sum_{p \in V} X^p V_p \quad (20)$$

where  $\langle X \rangle$  denotes the average of the quantity  $X$ ;  $X^p$  is the quantity of  $X$  pre-averaged at the single particle scale;  $V$  is the volume of the granular specimen that includes both the granular solids and the voids. Introducing the PSD function  $p(r)$  in Eq. (20), we can rewrite Eq. (20) in an integral form

$$\langle X \rangle = \frac{\overline{X^p V_p}}{(1+e)\overline{V_p}} \quad (21)$$

where  $e$  is the void ratio and  $\overline{\dots}$  denotes  $\int_{r_{\min}}^{r_{\max}} \dots p(r) dr$ . For the sake of simplicity, we use the notation  $\overline{X}$  instead of  $\langle X \rangle$  in the following if there is no ambiguity.

#### 3.2.1 Internal energy density

According to the volume averaging approach in Eq. (21), we can obtain the averaged hydrostatic stress  $\sigma_m$  of the granular system by integrating Eq. (9)

$$\sigma_m = \frac{\overline{C(r)f(r)r}}{4\pi(1+e)r^3} \quad (22)$$

Similarly, we can obtain the internal energy density for the granular system by integrating Eq. (15)

$$u = \frac{3\Omega}{10\pi(1+e)} \frac{\overline{r^{-1/3}[f(r)]^{5/3}C(r)}}{r^3} \quad (23)$$

where the coordination number  $C(r)$  is estimated using Eq. (18). We recall that the contact force  $f(r)$  is not yet determined.

There are some empirical relationships in the literature for the estimation of the contact forces in the granular media. However, adopting these empirical relationships will inevitably involve parameters that have no physical meanings. Here, an alternative method is adopted to estimate the contact force. For the sake of simplicity, we ignore the heterogeneity of the microscopic stress  $\sigma_m^p$ , which means

$$\sigma_m^p = \frac{C(r)f(r)}{4\pi r^2} = \text{const.}, \quad \forall r \in [r_{\min}, r_{\max}] \quad (24)$$

The above condition suggests that  $\sigma_m^p$  is independent of the particle size  $r$ . Adopting this condition and averaging the  $\sigma_m^p$  to the total volume yields

$$\sigma_m = \frac{\sigma_m^p}{1+e} \quad (25)$$

Substituting Eq. (24) into Eq. (25) eventually leads to

$$C(r)f(r) = 4\pi(1+e)\sigma_m r^2 \quad (26)$$

Equation (26) shows that for a given stress, the contact force in a polydisperse granular sample can be related to the coordination number, which has been estimated previously in Eq. (18). However, before adopting Eq. (26), we would now like to examine the validity of the hypothesis in Eq. (24). For this purpose, the isotropic compression test on a granular material is simulated using the DEM software PFC<sup>3d</sup> developed by Itasca Consulting Group [24]. The DEM specimen consists of 5000 frictionless spherical particles with five different sizes. The elastic contact modulus  $E_c$  of particles is chosen to be  $1 \times 10^8$  Pa and the particle-wall friction coefficient is set to be zero to minimize the boundary effect. In the simulation, the specimen is hydrostatically compressed under a pressure of 50 kPa. After the compression, the void ratio  $e$  of the specimen equals 0.592.

Figure 2 gives the DEM simulation results at the hydrostatic pressure of 50 kPa, in which Fig. 2a is the force chain distribution and Fig. 2b plots the relationship between  $f(r)C(r)$  and  $4\pi(1+e)r^2$ . It is clearly shown in Fig. 2b that there exists a proportional relationship between  $f(r)C(r)$  and  $4\pi(1+e)r^2$ . The slope  $k$  of the line that fits this relationship equals 46.7 kPa, which basically agrees with the applied hydrostatic pressure of 50 kPa. That is to say, despite the heterogeneous nature of granular materials [43], the variation of the particulate stress  $\sigma_m^p$  with the

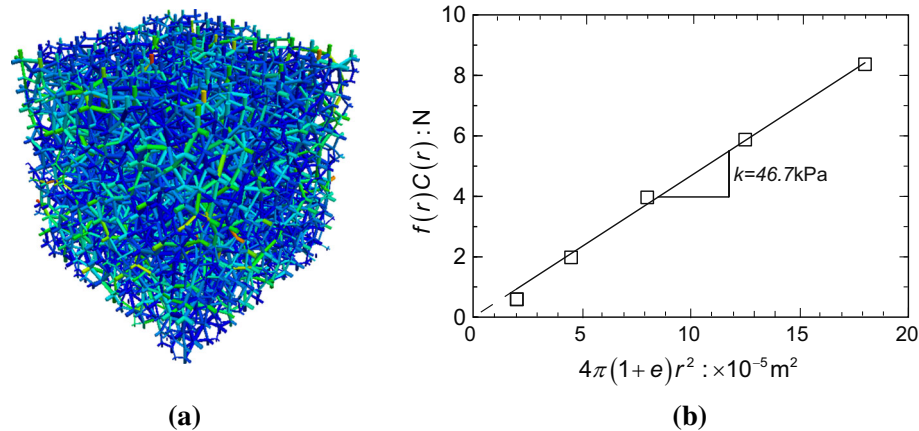


**Fig. 2** DEM simulation verification of the hypothesis of Eq. (24): **a** force chains distribution, **b**  $f(r)C(r)$  against  $4\pi(1+e)r^2$

particle size  $r$  is not significant. Thus, we consider that Eq. (26) is valid for polydisperse granular materials.

Substituting Eq. (26) into Eq. (23), we obtain the internal energy density of a granular system

$$u = [4\pi(1+e)]^{5/3} \frac{3\Omega}{10\pi(1+e)} \sigma_m^{5/3} \frac{r^3/[C(r)]^{2/3}}{r^3}. \quad (27)$$

### 3.2.2 Dissipative energy density

For a spherical particle, the volume  $V_p$  and the surface area per unit volume  $S^p$  are  $4\pi r^3/3$  and  $3/r$ , respectively. Combining Eqs. (19) and (21), we can obtain the dissipation energy density rate due to the particle breakage in a granular specimen of spherical particles

$$\dot{\Phi} = G_f \dot{S} = \frac{3}{1+e} G_f \frac{\partial \left( \frac{r^2}{r^3} \right)}{\partial r}. \quad (28)$$

## 4 Quantification of particle breakage

### 4.1 Limitations of the relative breakage indexes

The degradation of granular materials can be characterized by the evolution of the PSD. Many indexes have been proposed to quantify the particle breakage [26, 30, 31, 38], of which Hardin's relative breakage index  $B_r$  [26] is the most famous. In Hardin's  $B_r$ , it was assumed that all particles would be eventually crushed to the extent that no particles remain larger than 0.074 mm. However, this assumption contradicts the growing understanding that the ultimate PSD of a crushable granular material under sufficiently large pressure will tend toward a self-similar distribution [19, 39, 41]. For this reason, Einav [19] suggested the use of an arbitrary fractal distribution as the

ultimate PSD to modify the Hardin's  $B_r$ . Both the relative breakage indexes proposed by Hardin and Einav can be written in a general form

$$\Gamma = L(\Gamma_0, \Gamma_u, B_r) \quad (29)$$

where  $\Gamma$ ,  $\Gamma_0$  and  $\Gamma_u$  denote the current, initial and ultimate PSDs, respectively;  $B_r$  is the relative breakage index;  $L$  denotes a linear function. The advantage of Eq. (29) is that the current PSD can be quantified by a single scalar, i.e., the breakage index  $B_r$ , provided that the initial and ultimate PSDs are known. However, these definitions are limited because of the two following reasons:

1. The existence of a unique ultimate PSD is not clear. Based on the results of ring shear tests on a carbonate sand by Coop et al. [16], Einav [19] suggested the use of a fractal distribution with the fractal dimension of 2.59 as the ultimate PSD. This suggestion agreed basically with the study of Sammis et al. [50], who argued that the ultimate PSD should have a fractal dimension of 2.58 after the analysis of the fractal dimension of undisturbed fault gouges. However, the fractal dimension of the Apollonian packing, which is widely considered to be the idealized ultimate packing, is slightly smaller ( $D = 2.47$ ). In addition, the ultimate fractal dimension for coarse-grained materials may be greater than 2.6. For example, Du et al. [18] conducted compaction tests on a coarse-grained soil and found that the fractal dimension of the PSD was greater than 2.8; Wu et al. [57] statistically analyzed the fractal dimensions of a large number of rockfill materials in dams and found that most of them are greater than 2.6. In this context, it is doubtful whether there exists a unique ultimate PSD for an arbitrary crushable granular material under compression.
2. The influence of the PSD is not considered. The particle size has a great influence on the mechanical

behaviors of granular materials. For example, a uniform granular material composed of big particles presents more crushing than one composed of small particles with the same material properties [25, 26, 31]. As the relative breakage indexes are dimensionless, the effect of the PSD cannot be considered.

### 4.2 Indicator of particle breakage

In this study, instead of using a relative breakage index, we simply characterize the particle breakage by quantifying the change of the cumulated mass distribution (CMD). The following function is adopted to describe an arbitrary CMD

$$\frac{M_{(L<r)}}{M_T} = \frac{\Lambda^{3-D} - \lambda^{3-D}}{\Lambda^{3-D} - 1} \tag{30}$$

where  $M_{(L<r)}$  is the mass of particles with radius smaller than  $r$ ;  $M_T$  is the total mass of the granular system;  $\lambda = r/r_{max}$  and  $\Lambda = r_{min}/r_{max}$ , in which  $r$ ,  $r_{max}$  and  $r_{min}$  are the particle radius  $r$ , the maximum radius and minimum radius, respectively;  $D$  is a constant parameter. If  $r_{min}$  tends toward zero, the CMD becomes a fractal distribution and the parameter  $D$  is the fractal dimension of the CMD [41, 50, 55]. Figure 3 presents three typical CMDs based on Eq. (30) both in semi-log axes (Fig. 3a) and in log-log axes (Fig. 3b). It can be seen that these curves in Fig. 3b can be approximated by line segments. The determination of these line segments requires three characteristics: the particle size span, the maximum particle size and the slope of the CMD curve in log-log axes, which correspond to  $\Lambda$ ,  $r_{max}$  and  $3 - D$ , respectively.

Therefore, the indicator of particle breakage  $\Gamma$  in Eq. (2) can be quantified by the evolution of the three parameters ( $\Lambda$ ,  $r_{max}$  and  $D$ ). For the convenience's sake,  $\Gamma$  is written in the vectorial form

$$\Gamma_i = (r_{max}, \Lambda, D) \quad i = 1, 2, 3 \tag{31}$$

We remark that using Eq. (30) to describe the PSD of soils undergoing substantial crushing is not novel. However, Eq. (30) is rarely used to describe the amount of particle breakage because it does not include a predefined evolution path for the breakage. Thus, developing a breakage model using Eq. (30) requires better understanding of the physics of particle breakage.

For spherical particles with the uniform density, one can further obtain the particle number distribution function  $p(r)$  from Eq. (30) (see ‘‘Appendix’’)

$$p(r) = \frac{-D}{r_{max}(1 - \Lambda^{-D})} \lambda^{-1-D} \tag{32}$$

## 5 Complete elastic-breakage model

### 5.1 Model formulation

By now, we have established the overall thermomechanical framework for the isotropic compression of crushable granular materials. Micromechanically based expressions for the energy densities of frictionless granular materials under isotropic compression have been formulated. In addition, we have also proposed the function to describe an arbitrary PSD and the indicator to quantify particle breakage. In what follows, we will establish an elastic-breakage compression model, where emphasis is placed on determining the evolution of the particle breakage.

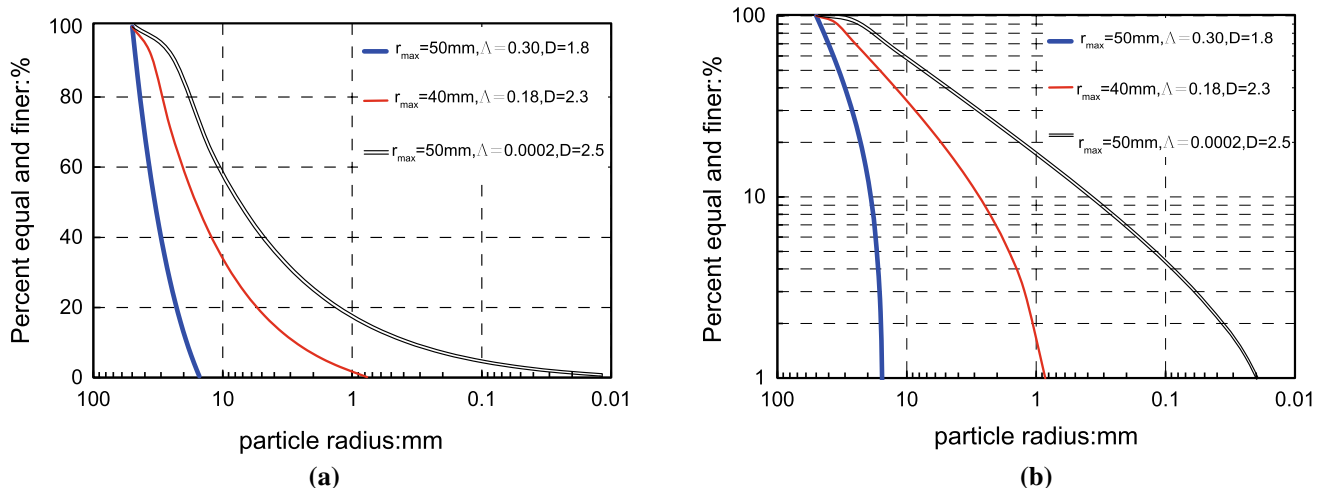


Fig. 3 Three typical CMDs of granular soils in: **a** semi-logarithmic axes, **b** double logarithmic axes

### 5.1.1 Energy densities

Although the internal and frictional energy densities are formulated in Eqs. (27) and (28), the PSD was not specified in the two equations. By substituting Eqs. (18) and (32) into Eq. (27), we can rewrite the internal energy density with specified PSD

$$u = \Theta \sigma_m^{5/3} \eta(A, D) \quad (33)$$

where  $\Theta$  depends on the material properties of particles and the compactness of the granular system, given by

$$\Theta = \frac{6}{5} \sqrt[3]{4\Omega(\pi c_s)^{2/3}(1+e)^{2/3}} \quad (34)$$

$H$  is given as follows

$$\eta(A, D) = \frac{\left(\frac{-D}{1-A^D}\right)^{2/3} \int_A^1 \lambda^{2-D} \left( \int_A^1 \left(1 - \sqrt{\frac{2\lambda'\lambda + \lambda^2}{(\lambda + \lambda')^2}}\right) \lambda'^{-1-D} d\lambda' \right)^{2/3} d\lambda}{\int_A^1 \lambda^{2-D} d\lambda} \quad (35)$$

Similarly, the rate of the dissipative energy density with specified PSD is obtained by combining Eqs. (28) and (32)

$$\dot{\Phi} = \frac{G_f}{1+e} \dot{S}(r_{\max}, A, D) \quad (36)$$

where  $S$  is given by

$$S = 3 \frac{3 - D1 - A^{2-D}}{2 - D1 - A^{3-D}} \frac{1}{r_{\max}} \quad (37)$$

It is noted from Eqs. (33)–(37) that the internal energy density is independent of the maximum particle size  $r_{\max}$ , while the rate of the dissipative energy density is proportional to  $1/r_{\max}$ .

### 5.1.2 Elastic compression

Combing Eqs. (5) and (33), we obtain the expression for the elastic bulk modulus

$$K_B^c = \frac{3}{5\Theta\eta} \sigma_m^{1/3} \quad (38)$$

As the elastic bulk modulus  $K_B^c$  can be related to the void ratio  $e$  according to its definition, Eq. (38) can also be rewritten in the following differential form

$$-\frac{de}{1+e} = \frac{5}{3} \Theta \eta \sigma_m^{-1/3} d\sigma_m \quad (39)$$

### 5.1.3 Evolution of particle breakage

We term  $\chi_i$  as the “dissipative breakage energy gradient” that describes the energy releasing due to per unit of the particle breakage indicator  $\Gamma$ , and  $\bar{\chi}_i$  the “breakage energy gradient” describing the energy dissipated due to per unit of particle breakage indicator, which are defined as

$$\chi_i = \frac{\partial \dot{\Phi}}{\partial \dot{\Gamma}_i}, \quad \bar{\chi}_i = \frac{\partial u}{\partial \Gamma_i} \quad (40)$$

The rate of the dissipative energy density given in Eqs. (36) and (37) indicates that for a rate-independent material, the dissipation rate is a homogenous first-order function in the breakage rate  $\dot{\Gamma}$ . In other words, the magnitude of dissipated energy rate must be directly proportional to the magnitude of particle breakage rate. The Euler’s theorem for a homogenous function gives

$$\frac{\partial \dot{\Phi}}{\partial \dot{\Gamma}} \dot{\Gamma} = \dot{\Phi} \quad (41)$$

Substituting Eqs. (40) and (41) into Eq. (6), one can rewrite the energy conservation equation as

$$(\chi_i + \bar{\chi}_i) \dot{\Gamma}_i = 0 \quad (42)$$

It is noted that unlike the scalar relative breakage indexes, the breakage indicator here  $\dot{\Gamma}$  is a vector with three degrees of freedom:  $r_{\max}$ ,  $A$  and  $D$ . As a result, the choice of the breakage indicator with more than one degrees of freedom here may make a significant difference in Eq. (42): Since  $\dot{\Gamma}$  is a vector, Eq. (42) only implies that  $(\chi_i + \bar{\chi}_i)$  is orthogonal to  $\dot{\Gamma}_i$ . Hence, additional information is needed to determine the evolution of the breakage. However, Ziegler [63] argued that a much stronger statement  $(\chi_i + \bar{\chi}_i) = 0$  can be made based on the hypothesis of maximum dissipation. Although Ziegler’s condition is debatable, it is sufficiently wide to provide realistic descriptions of many materials, including some that involve dissipation which depends on the applied pressure and (in the terminology of plasticity theory) non-associated flow [28]. Here, we adopt Ziegler’s condition and then Eq. (42) becomes

$$(\chi_i + \bar{\chi}_i) = 0 \quad (43)$$

With the Ziegler’s condition (maximum dissipation principle), the evolution path of the PSD can be determined. Noting that the internal energy density is size-independent, i.e.,  $\partial u / \partial r_{\max} = 0$ , we can derive from Eq. (43) that  $\partial \dot{\Phi} / \partial \dot{r}_{\max} = 0$ . This result implies that although  $r_{\max}$  is allowed to evolve in the definition of the breakage indicator  $\Gamma_i$  during particle breakage, the maximum dissipation principle requires it to remain unchanged. The invariance of  $r_{\max}$  can be supported by the results of many experimental results of compression of crushable granular

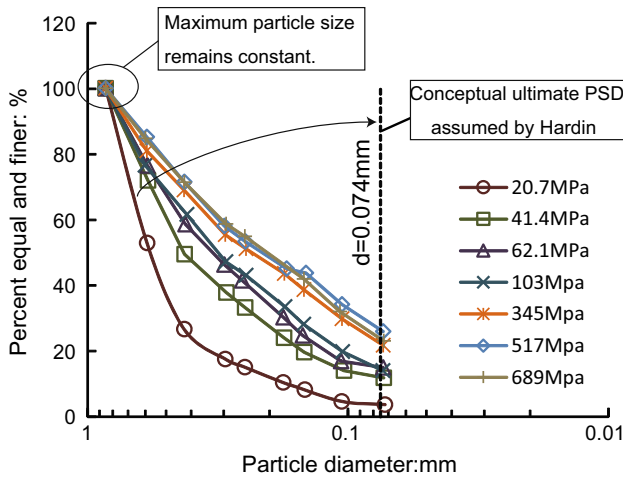


**Fig. 4** Evolution of PSDs for Black beauty slag under high compressive pressure by Hagerty et al. [25]

materials. For instance, Fig. 4 shows the high-pressure compression tests on Black beauty slag by Hagerty et al. [25]. Although sands underwent substantial crushing during the test, as observed from the evolution of the PSD, the maximum particle size remain almost unchanged. This result also explains why not particles are crushed to the extent that no particles remain larger than a cut-off size (0.074 mm), as was assumed by Hardin [26]. As  $r_{max}$  remains constant during breakage, the particle breakage indicator  $\Gamma_i$  is degenerated into

$$\Gamma_i = (A, D) \tag{44}$$

The roles of the particle breakage rate  $\dot{\Gamma}_i$  and the dissipative particle breakage gradient  $\chi_i$  can be interchanged through a Legendre transformation, as was discussed by Collin and Houlsby [14]. As the dissipation is homogenous and first-order in  $\dot{\Gamma}_i$ , the degenerate special case of the Legendre transformation leads to a function of  $\chi_i$ . Collin and Houlsby [14] argued that as this function is identically zero, it is none other than the yield function. Thus, from Eqs. (36), (37) and (43), we can write the yield function  $y_B(\chi_i)$  as

$$\lambda_B y_B \equiv F_i \chi_i - G_f = 0 \tag{45}$$

where for convenience, we designate  $F_i = (1 + e)/(\partial S/\partial \Gamma_i)$  and  $\lambda_B$  is a nonnegative multiplier.

The Legendre transformation of Eq. (45) leads to the flow rule

$$\dot{\Gamma}_i = \lambda_B \frac{\partial y_B}{\partial \chi_i} = \lambda_B F_i \tag{46}$$

Differentiating Eq. (45) yields

$$F_i \dot{\chi}_i + \frac{\partial F_i}{\partial \Gamma_j} \dot{\Gamma}_j \chi_i = 0 \tag{47}$$

Combining Eqs. (40) and (43), we can obtain

$$\chi_i = -\dot{\chi}_i = -\frac{\partial u}{\partial \Gamma_i} \tag{48}$$

Since the internal energy is a function of the stress and the PSD, denoted as  $u(\sigma_m, \Gamma_i)$ , differentiating Eq. (48) yields

$$\dot{\chi}_i = -\frac{\partial^2 u}{\partial \Gamma_i \partial \Gamma_j} \dot{\Gamma}_j - \frac{\partial^2 u}{\partial \Gamma_i \partial \sigma_m} \dot{\sigma}_m \tag{49}$$

Consequently, one can obtain the multiplier  $\lambda_B$  by substituting Eqs. (46) and (49) into Eq. (47)

$$\lambda_B = -\frac{F_i \frac{\partial^2 u}{\partial \Gamma_i \partial \sigma_m} \dot{\sigma}_m}{F_i \frac{\partial^2 u}{\partial \Gamma_i \partial \Gamma_j} F_j + \frac{\partial u}{\partial \Gamma_i} \frac{\partial F_i}{\partial B_j} F_j} \tag{50}$$

During particle breakage, the stress–strain relation for isotropic compression of granular materials can also be described using Eq. (39) because the plastic strain is not considered in this study, as mentioned previously. However, in contrast to the elastic compression where the parameter  $\eta(A, D)$  is constant, the particle breakage stage is accompanied by the evolution of  $\eta(A, D)$ . Thus, the stress–strain relation during particle breakage stage should be calculated by considering the evolution of  $\eta(A, D)$ .

### 5.1.4 Summary of the model

The complete elastic-breakage model for the compression of crushable granular materials is summarized in Table 1. Although this model seems more complex compared with the existing breakage theories (e.g., Einav [19–22], McDowell and Bolton [7, 39, 41]), it contains only three basic material parameters (Young’s modulus  $E$ , Poisson’s ratio  $\nu$  and the strain energy release rate  $G_f$ ) of particles and one fabric related parameter (the linear capacity  $c_s$ ). Moreover, as the model is derived purely on the basis of the micro–macro averaging and the laws of thermodynamics without any empirical relations, it predicts, rather than depicts the behavior of particle breakage.

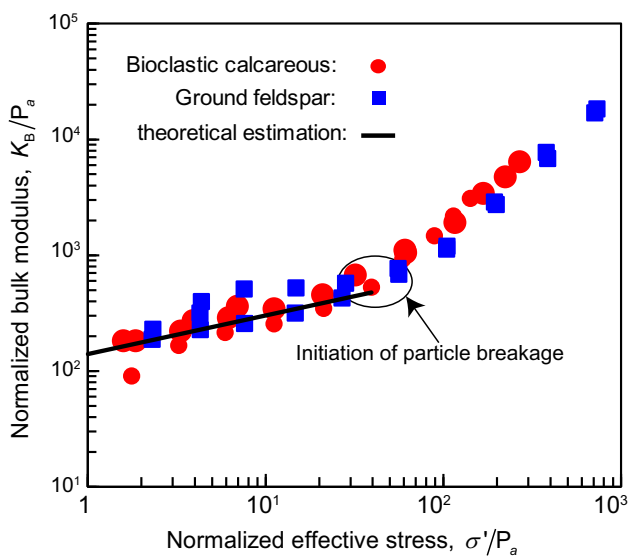
## 5.2 Model performance

### 5.2.1 Elastic compression stage

The model prediction for the elastic stage in comparison with the experimental data from [47] is illustrated in Fig. 5. The bulk modulus  $K_B$  of two different sands (bioclastic calcareous and ground feldspar) is plotted against the effective stress  $\sigma'$  in log–log axes, where both  $K_B$  and  $\sigma'$  are normalized by the atmosphere pressure  $p_a$ . The relationship between  $K_B/p_a$  and  $\sigma'/p_a$  depicted in Fig. 5 shows an apparent change of the trend at the pressure of around

**Table 1** Complete elastic-breakage model for compression of crushable granular materials

Variables	
Breakage indicator	$\Gamma_i = (A, D)$
Internal energy density	$u = \Theta \sigma_m^{5/3} \eta(A, D)$
	$\Theta = \frac{6}{5} \sqrt[3]{4\Omega} (\pi c_s)^{2/3} (1+e)^{2/3}$
	$\eta(A, D) = \frac{\left(\frac{-D}{1-A-D}\right)^{2/3} \int_A^1 \lambda^{2-D} \left( \int_A^1 \left(1 - \sqrt{\frac{2\lambda' \lambda + \lambda'^2}{(\lambda+\lambda')^2}}\right) \lambda'^{-1-D} d\lambda' \right)^{2/3} d\lambda}{\int_A^1 \lambda^{2-D} d\lambda}$
Dissipative energy density	$\dot{\Phi} = \frac{G_t}{1+e} \dot{S}(r_{\max}, A, D)$
	$S = 3 \frac{3-D}{2-D} \frac{1-A^{2-D}}{1-A^{3-D}} \frac{1}{r_{\max}}$
	$F_i = (1+e)/(\partial S/\partial \Gamma_i)$
Yield criterion	
$F_i \lambda_i - G_t < 0$ , elastic	$F_i \lambda_i - G_t = 0$ , breakage
Evolution of PSDs	
$\dot{\Gamma}_i = 0$	$\dot{\Gamma}_k = - \frac{F_i \frac{\partial^2 u}{\partial \Gamma_i \partial \sigma_m} \dot{\sigma}_m}{F_i \frac{\partial^2 u}{\partial \Gamma_i \partial \Gamma_j} F_j + \frac{\partial u}{\partial \Gamma_i} \frac{\partial F_i}{\partial B_j} F_j} F_k$
Stress–strain	
$-\frac{de}{1+e} = \frac{5}{3} \Theta \eta \sigma_m^{-1/3} d\sigma_m$ , where $\eta$ is a constant	$-\frac{de}{1+e} = \frac{5}{3} \Theta \eta \sigma_m^{-1/3} d\sigma_m$ , where $\eta$ should be coupled with the calculation of breakage

**Fig. 5** Theoretically predicted bulk modulus against the effective stress compared with experimental results from [47]

6 MPa, indicating the initiation of the particle breakage. The straight line in Fig. 5 is the theoretical prediction of the elastic compression (before 6 MPa) using Eq. (38). As implied by Eq. (38), the bulk modulus of for the elastic compression is proportional to  $\sigma_m^{1/3}$ , which should corresponds to a straight line with a slope of 1/3 in log–log axes. As can be seen in Fig. 5, the theoretically predicted line follows the same trends against the applied stress as the experimental results. The same conclusion that the bulk

modulus is proportional to  $\sigma_m^{1/3}$  was also found in [10] and adopted in the compression model of cohesionless soils in [47].

The effect of the PSDs on the bulk modulus of granular materials is predicted using Eq. (38). As mentioned previously, the PSD is characterized by the parameter  $A (= r_{\min}/r_{\max})$  and the fractal dimension  $D$ . Figure 6 presents the predicted influence of  $A$  and  $D$  on the bulk modulus. To avoid the influence of the material property ( $\Theta$ ) and the stress ( $\sigma_m$ ), the bulk modulus  $K_B$  in the figure is multiplied by the factor  $\Theta/\sigma_m^{1/3}$  according to Eq. (38). As seen in Fig. 6a, the decrease of  $A$  (increase of the polydispersity) results in the increase of the bulk modulus, probably because smaller particles lead to less uniformity of the contact forces. Figure 6b gives the variation of  $K_B \Theta/\sigma_m^{1/3}$  by theoretical prediction with the fractal dimension  $D$  for  $A=0.1$ . It increases as the value of  $D$  increases initially and decreases afterward. The maximum value of  $K_B \Theta/\sigma_m^{1/3}$  is attained at  $D \approx 1.65$ . A similar variation trend was found in the DEM simulation of compression tests on granular samples with the same  $A = 0.1$  by Minh and Cheng [43] (see Fig. 6b). In the simulation,  $1/C_c$  was used to reflect the rigidity of the materials, which is qualitatively equivalent to  $\Theta K_B/\sigma_m^{1/3}$ .  $1/C_c$  attains its maximum value at  $D \approx 2.1$ . It is commonly recognized that the fractal dimension  $D$  corresponding to the ultimate PSD of crushable granular materials is about 2.59. Here, both the theoretical prediction and the DEM simulation imply the existence of another characteristic fractal

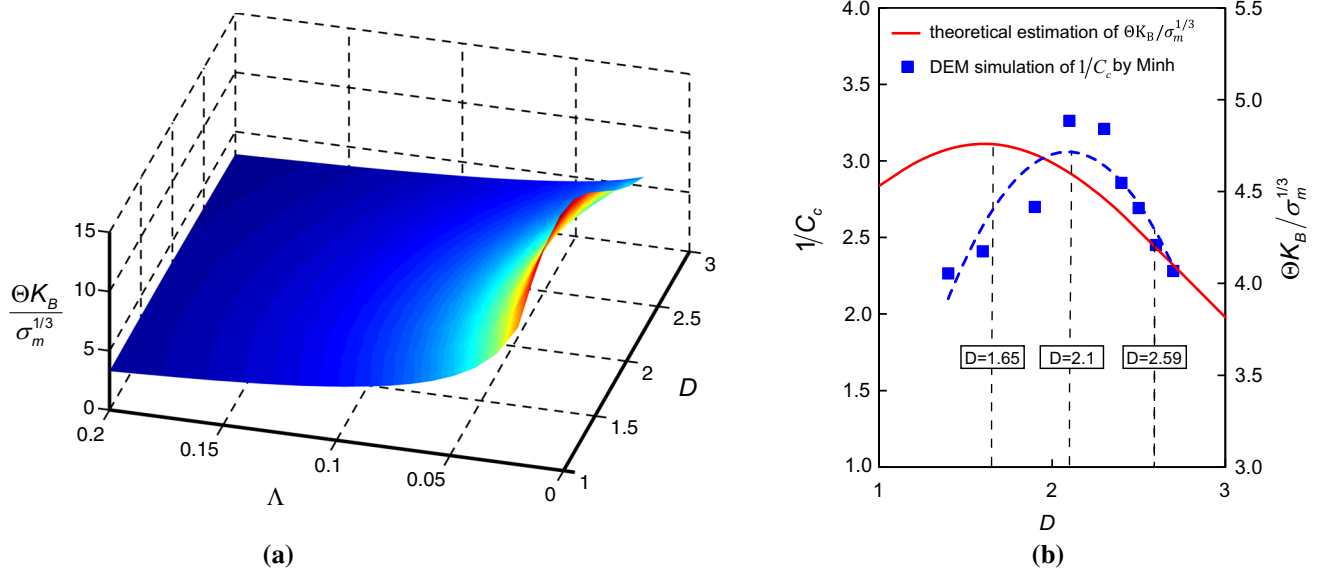


**Fig. 6** Influence of the PSDs on the bulk modulus: **a** predicted bulk modulus against  $\Lambda$  and  $D$ , **b** comparison of the predicted and simulated elastic compressibility of granular materials with different fractal dimensions

dimension of the PSD, which corresponds to the maximum value of the bulk modulus.

### 5.2.2 The yielding stress

Substituting Eqs. (33), (37) and (40) into the yield function Eq. (45), one can obtain the yield stress  $\sigma_f$  as

$$\sigma_f = \left( -\frac{G_f}{\Theta H_i \frac{\partial \eta}{\partial I_i}} \right)^{3/5} (r_{\max})^{-3/5} \tag{51}$$

where we designate  $F(r_{\max}, \Lambda, D) = H(\Lambda, D)r_{\max}$  for convenience. Equation (51) indicates that the yield stress  $\sigma_f$  depends on the properties of the grain material ( $G_f$  and  $\Theta$ ) and the PSD of the granular material (represented by  $H_i$ ,  $\eta$  and  $r_{\max}$ ). Equation (51) also implies that the yielding stress  $\sigma_f$  is size-dependent with  $\sigma_f \propto r_{\max}^{-3/5}$ . In other words, the relationship between  $\sigma_f$  and  $r_{\max}$  can be represented by a straight line with a slope of  $-3/5$  in log–log scales. Figure 7 presents the results of single particle crushing tests on three batches of silica sand grains and one batch of Toyoura sand grains of different sizes performed by Nakata et al. [45], together with the theoretical prediction using Eq. (51) in log–log axes. As can be seen, the experimental data is basically predicted by Eq. (51). In fact, Eq. (51) reflects the upscaling law for the breakage of granular materials. Similar upscaling laws were also obtained by Zhang et al. [60], who interpreted the size dependence of the yielding for single particles using fracture mechanics, breakage mechanics and Weibull statistics. As the upscaling law in Eq. (51) is derived from a granular assembly with an arbitrary PSD, it may be regarded as an extension

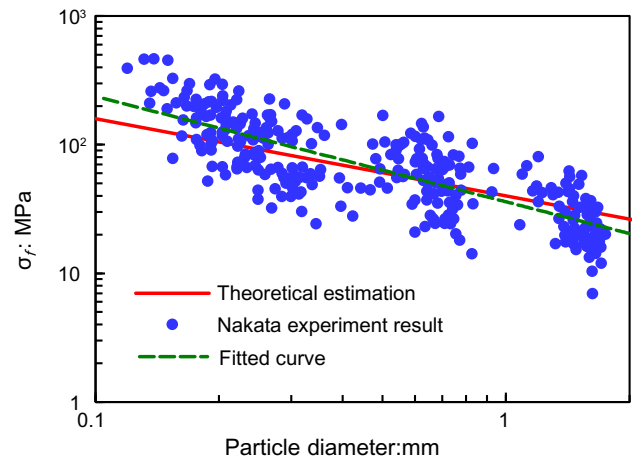


**Fig. 7** Results of single particle crushing tests by Nakata et al. versus the theoretical prediction

from a single particle scale to a granular assembly scale. This result may provide a theoretical basis to estimate the effect of widely variable particle sizes in large-scale applications for which direct testing is not feasible, such as rockfill engineering and mining technologies.

Figure 8 shows the effect of the polydispersity ( $\Lambda$ ) and the fractal dimension ( $D$ ) of the PSD on the yielding stress estimated using Eq. (51). To avoid the influence of material properties ( $G_f$  and  $\Theta$ ) and the maximum particle size ( $r_{\max}$ ), the yielding stress  $\sigma_f$  in the figure is multiplied by the factor  $(r_{\max} \Theta / G_f)^{3/5}$  according to Eq. (51). The estimated results indicate that in the case of narrow-size distribution with higher value of  $\Lambda (\Lambda \rightarrow 1)$ , the yielding

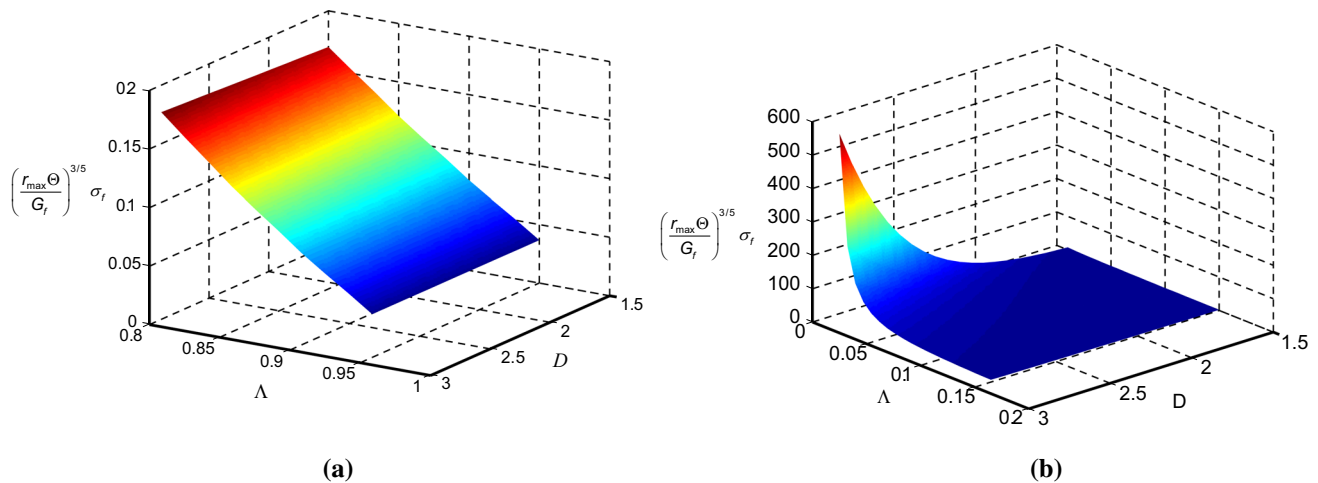


**Fig. 8** Prediction of the effect of PSDs on the yield stress for: **a** narrow-size distribution, **b** highly polydisperse distribution

stress is governed mainly by the polydispersity (see Fig. 8a), increasing almost linearly with the decrease of  $\Lambda$  (increase of polydispersity). In this case, the effect of the fractal dimension  $D$  is nonsignificant compared with  $\Lambda$ . However, in the case of highly polydisperse distribution with smaller value of  $\Lambda$  ( $\Lambda \rightarrow 0$ ), the yielding stress increases significantly with the increasing polydispersity (decreasing  $\Lambda$ ) as well as the fractal dimension  $D$ , as shown in Fig. 8b. It can be observed from Fig. 8b that when the fractal dimension reaches a sufficiently large value in the case of polydisperse distribution, the yielding stress increase abruptly, implying that further change of the PSD requires much greater compressive pressure. It is probably for this reason that the particle breakage can be attenuated even under sufficiently great pressure.

### 5.2.3 Evolution of PSD and void ratio during particle breakage

The evolution of the PSDs of the Black Beauty slag under one-dimensional high-compression by Hagerty et al. [25], as given in Fig. 4, can be predicted by using the elastic-breakage model proposed in this study. In the prediction, the Young's modulus and the Poisson's ratio of grain materials are chosen to be  $E = 100$  GPa and  $\nu = 0.09$ , respectively, in accordance with the order of magnitude of rock materials. The linear capacity  $c_s$  of polydisperse granular materials is taken as a constant value of 3.0 based on the DEM simulation results performed in Sect. 3.2. With these model parameters, the bulk modulus is theoretically estimated to be 237 MPa for  $\sigma_m = 2$  MPa, which basically agrees with the one-dimensional compression test results reported in [25] assuming the lateral/vertical stress ratio  $K_0 = 0.4$ . The strain energy release rate  $G_f$  is chosen to be  $300$  J/m<sup>2</sup>, with which the calculated yielding stress

$\sigma_f = 18$  MPa is close to the experimental results of Black Beauty slag in [25]. The predicted evolution of the PSDs for Black Beauty slag is presented in Fig. 9, which agrees basically with the experimental data. Figure 9 also plots the evolution of the fractal dimension  $D$  against the applied stress. As can be seen, the fractal dimension  $D$  increases with the increasing stress and this trend gradually slows down, also in accordance with the experimental results. Here, we would like to recall that unlike in the theory of breakage mechanics which predefines the evolution path of the PSD [19], the evolution of the PSD in the proposed model is purely determined using micromechanics and thermomechanics. Given such consideration, the model prediction is quite good.

Figure 10 gives the predicted evolution of the void ratio  $e$  against the applied stress  $\sigma_m$  (compression curve). As the

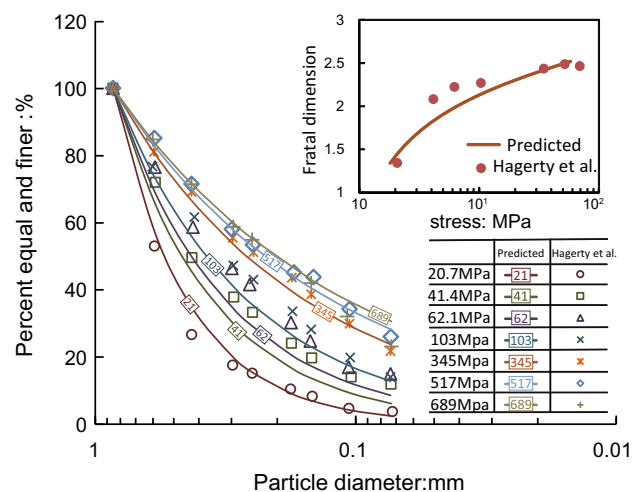


**Fig. 9** Comparison between the predicted PSD evolution and test results of Black beauty slag by Hagerty et al. [25]

elastic-breakage model does not account for the plastic deformation, the theoretically predicted compression curve is not compared with the experimental data. However, the predicted evolution of the void ratio against the applied stress follows the same overall trend as obtained from experiments on crushable soils (e.g., [25, 59]). It consists of three phases: the elastic compression, breakage stage and the pseudoelastic stage. During the elastic compression phase, no particle breakage takes place. When the applied stress reaches the yielding stress, the particle breakage occurs and continues until a pseudoelastic phase where the evolution of the PSD becomes nonsignificant, accompanying with the little change of the void ratio.

## 6 Discussion on generalization of the model

Despite the thermomechanical and micromechanical insight provided, the proposed model is only suitable for isotropic and elastic-breakage problems. In real cases, particle breakage is often accompanied with particle rearrangements, subsequently resulting in plastic deformation and additional dissipation of energy, designated as  $\dot{\Phi}^P$ . Moreover, the particle breakage may take place not only under compression, but also during shearing. Generalization of the proposed breakage model from isotropic compression to more general stress states may lay an important foundation for the physically based constitutive modeling of granular materials incorporating particle breakage. Here, rather than give a detailed solution, we point out a possible way to consider the plastic dissipation and the generalized stress state.

The plastic dissipation may be considered in the thermodynamics statement for isotropic compression as

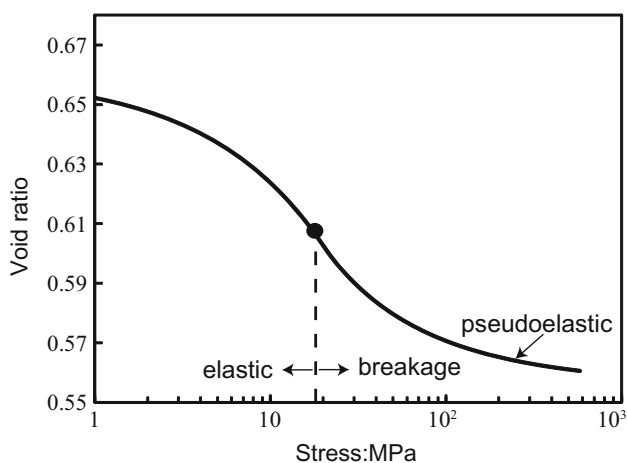


**Fig. 10** Stress–void ratio relationship predicted by the proposed elastic-breakage model

$$\sigma_m(\dot{\epsilon}_v^e + \dot{\epsilon}_v^p) = \dot{u} + (\dot{\Phi} + \dot{\Phi}^P) \quad (52)$$

That is to say, the total dissipation is divided into two additive parts: the plastic dissipation  $\dot{\Phi}^P$  and the dissipation due to particle breakage  $\dot{\Phi}$ , although the additivity of  $\dot{\Phi}^P$  and  $\dot{\Phi}$  is still a matter of debate. Less trivial form considering the coupling of plastic-breakage dissipation was discussed in [20].

In general, the plastic dissipation is a function of the breakage indicator  $\Gamma$  and the plastic strain  $\dot{\epsilon}_v^p$  expressed as

$$\dot{\Phi}^P = \dot{\Phi}^P(\Gamma, \dot{\epsilon}_v^p) \quad (53)$$

The expressions for the internal energy and the dissipation due to particle breakage remain unchanged, given in Eqs. (2) and (3). Substituting Eqs. (2), (3) into Eq. (52) yields

$$\left( \sigma_m / K_B^e - \frac{\partial u}{\partial \sigma_m} \right) \dot{\sigma}_m = \left( \frac{\partial u}{\partial \Gamma} \dot{\Gamma} + \dot{\Phi} \right) + (\dot{\Phi}^P - \sigma_m \dot{\epsilon}_v^p) \quad (53)$$

Similar to the elastic-breakage formulation, all the terms in the three brackets should be equal to zero, which means that the elastic–plastic-breakage problem can be decoupled into three independent problems. Hence, in addition to Eqs. (5) and (6), one has

$$\dot{\Phi}^P - \sigma_m \dot{\epsilon}_v^p = 0 \quad (54)$$

In light of the thermomechanical formulation, the plastic deformation can be taken into account if we can formulate a concrete expression for the plastic dissipation defined in Eq. (53). Of course, we could formulate a plastic dissipation through the micro–macro procedure, as performed in Sect. 3. For instance, the work of Zhao et al. [61] has shed lights on such formulation. Here, a less rigorous but simpler alternative of estimating the plastic dissipation is proposed by analogy with the frictional dissipation energy at two contacted surfaces. As the frictional dissipation at two contacted surfaces is proportional to the normal contact force and the sliding displacement, the plastic dissipation for granular materials is expressed as

$$\dot{\Phi}^P = \mu \sigma_m S \dot{\epsilon}_v^p \quad (55)$$

where  $S$  is the averaged surface per unit volume defined in Sect. 3, which can be related to the breakage indicator  $\Gamma$  via Eq. (28);  $\mu$  is a material constant related to the inter-particle friction coefficient.

Once the elastic–plastic-breakage model is developed for isotropic compression, extrapolation to more generalized stress state may be completed within the framework of critical state soil mechanics (see the work by Roscoe and Burland [49]). In order to account for the influence of particle breakage, the dissipation due to breakage  $\dot{\Phi}$  is

added in the original work equation by Roscoe and Burland, expressed as

$$p' \dot{\epsilon}_v^p + q \dot{\epsilon}_s^p = \dot{\Phi}^p + \dot{\Phi} \quad (56)$$

where  $p'$  is the mean effective stress and  $\dot{\epsilon}_s^p$  is the plastic shearing strain. In isotropic compression, we have  $p' = \sigma_m$ . Details to formulate the constitutive relationship from the work equation can refer to [14, 15].

## 7 Conclusion

A micromechanically based model for the compression of crushable granular materials was established in the framework of thermomechanics. In this model, no empirical relationship is adopted. Both the internal and dissipative energies were derived using the micro–macro volume averaging approach. The energy dissipation due to particle breakage was directly related to the evolution of the PSD, which was quantified by three parameters: the particle size  $r_{\max}$ , the polydispersity  $\lambda$  and the fractal dimension  $D$ . It is demonstrated that without a predefined evolution path of the PSD, the yielding and the evolution of the breakage can be determined by the maximum dissipation principle in the framework of thermomechanics. The developed model contains three material parameters that have concrete physical meanings: (Young's modulus, Poisson's ratio and the strain energy release rate) of the composing particles and one fabric related constant (the linear capacity) of the granular system. By using the proposed model, the evolution of the PSD as well as the void ratio of granular material can be predicted without any empirical results.

The model was used to investigate the bulk modulus, the yielding stress as well as the evolution of the PSD and the void ratio of crushable granular materials under compression. The results were compared with the experimental and DEM simulated results in the literature. The following remarks can be made:

1. Under elastic compression, the bulk modulus of granular materials is related to both the applied stress and the PSD. It is proportional to  $\sigma_m^{1/3}$  and increases with the increasing polydispersity of the PSD. The elastic bulk modulus increases as the fractal dimension  $D$  increases initially and decreases afterward, implying the existence of a fractal dimension of the PSD which corresponds to the maximum value of the bulk modulus.
2. The yielding stress  $\sigma_f$  of crushable granular materials under compression is size-dependent with  $\sigma_f \propto r_{\max}^{-3/5}$ . As this upscaling law was derived for a granular assembly with an arbitrary PSD, it might be regarded as an extension from a single particle scale to a

granular assembly scale. The yielding stress is also influenced by the polydispersity and the fractal dimension of the PSD. In the case of narrow-size distribution, the yielding stress is governed mainly by the polydispersity and is insensitive to the fractal dimension, whereas  $\sigma_f$  increases significantly with the increasing polydispersity and the fractal dimension in the case of highly polydisperse distribution.

3. The prediction of the evolution of the PSD using the proposed model does not need to predefine an evolution path since it is purely determined on the basis of the thermomechanics and the principle of maximum dissipation. Although the proposed elastic-breakage model cannot predict excellently the compression curve (i.e.,  $e-\sigma_m$  relationship) of crushable granular materials, it is capable of predicting the existence of the elastic-breakage-pseudoelastic compression phases.

**Acknowledgements** This work is supported by the “National Key R&D Program of China” (Grant No. 2017YFC0404800), the “National Natural Science Foundation of China” (Grant No. U1765205) and “the Fundamental Research Funds for the Central Universities” (Grant No. 2018B40914). Financial support from the National Natural Science Foundation of China (Project No. 51509077) and the Fundamental Research Funds for the Central Universities (Project No. 2016B03514) are also gratefully acknowledged.

## Appendix: Relationship between CMD and particle number distribution

The cumulated mass distribution (CMD), denoted here as  $\varphi(r)$ , is commonly used in geotechnical engineering to reflect the PSD of soils. It is defined as the percentage of mass equal and finer against the particle size

$$\varphi(r) = \frac{M_{(L \leq r)}}{M_T} \quad (57)$$

where  $M_{(L < r)}$  is the mass of particles with radius smaller than  $r$ ;  $M_T$  is the total mass of the granular sample.

An alternative description to reflect the PSD is the particle number distribution, defined as

$$p(r) = \frac{dN_{(L \leq r)}}{N_T dr} \quad (58)$$

where  $N_{(L \leq r)}$  is the number of particles with radius equal and smaller than  $r$ , and  $N_T$  is the total number of particles. According to Eq. (57), the mass fraction of particles with radius falling within the interval  $[r, r + dr]$  is  $d\varphi(r)$ . The number of particles corresponding to this mass fraction is thus calculated to be

$$dN(L \leq r) = \frac{M_T d\varphi(r)}{\rho V(r)} \quad (59)$$

where  $\rho$  is the density of the grain material and  $V(r)$  is the volume of a single particle with radius  $r$ . For spherical particles, we have

$$V(r) = \frac{4}{3} \pi r^3 \quad (60)$$

Based on Eq. (59), the total particle number  $N_T$  is easily integrated to be

$$N_T = \int_{r_{\min}}^{r_{\max}} dN(L \leq r) = \int_{r_{\min}}^{r_{\max}} \frac{M_T}{\rho V(r)} \frac{d\varphi(r)}{dr} dr \quad (61)$$

Substituting Eqs. (59) and (61) into Eq. (58) yields

$$p(r) = \frac{d\varphi(r)}{dr} \bigg/ V(r) \int_{r_{\min}}^{r_{\max}} \frac{1}{V(r)} \frac{d\varphi(r)}{dr} dr \quad (62)$$

Equation (62) establishes the relationship between the CMD, i.e.,  $\varphi(r)$ , and the particle number distribution  $p(r)$ .

Substituting the CMD in Eq. (30) into Eq. (62) and combining Eq. (60), one can obtain the particle number distribution  $p(r)$  as given in Eq. (32).

## References

- Alikarami R, Andò E, Gkiousas-Kapnisis M, Torabi A, Viggiani G (2015) Strain localisation and grain breakage in sand under shearing at high mean stress: insights from in situ X-ray tomography. *Acta Geotech* 10(1):15–30
- Alonso E, Olivella S, Pinyol N (2005) A review of Beliche Dam. *Géotechnique* 55(4):267–285
- Alonso E, Tapias M, Gili J (2012) Scale effects in rockfill behaviour. *Géotech Lett* 2(3):155–160
- Åström J, Herrmann H (1998) Fragmentation of grains in a two-dimensional packing. *Eur Phys J B Condens Matter Complex Syst* 5(3):551–554
- Bauer E (1996) Calibration of a comprehensive hypoplastic model for granular materials. *Soils Found* 36(1):13–26
- Ben-Nun O, Einav I, Tordesillas A (2010) Force attractor in confined comminution of granular materials. *Phys Rev Lett* 104(10):108001
- Bolton M, McDowell G (1997) Clastic mechanics. *Solid Mech Appl* 53:35–46
- Bolton M, Nakata Y, Cheng Y (2008) Micro- and macro-mechanical behaviour of DEM crushable materials. *Géotechnique* 58(6):471–480
- Bruchmüller J, Van Wachem B, Gu S, Luo K (2011) Modelling discrete fragmentation of brittle particles. *Powder Technol* 208(3):731–739
- Chang CS, Kabir MG, Chung Y (1992) Micromechanics modeling for stress-strain behavior of granular soils. II: evaluation. *J Geotech Eng* 118(12):1975–1992
- Cheng Y, Nakata Y, Bolton M (2003) Discrete element simulation of crushable soil. *Geotechnique* 53(7):633–641
- Ciantia M, Alvarez Arroyo, de Toledo M, Calvetti F, Gens Solé A (2015) An approach to enhance efficiency of DEM modelling of soils with crushable grains. *Géotechnique* 65(2):91–110
- Cil M, Alshibli K (2012) 3D assessment of fracture of sand particles using discrete element method. *Géotech Lett* 2(3):161–166
- Collins I, Houlsby G (1997) Application of thermomechanical principles to the modelling of geotechnical materials. In: *Proceedings of the Royal Society of London A Mathematical, Physical and Engineering Sciences*, vol 1964. The Royal Society, pp 1975–2001
- Collins IF, Muhunthan B (2003) On the relationship between stress–dilatancy, anisotropy, and plastic dissipation for granular materials. *Geotechnique* 53(7):611–618
- Coop M, Sorensen K, Freitas TB, Georgoutsos G (2004) Particle breakage during shearing of a carbonate sand. *Géotechnique* 54(3):157–164
- Das A, Bajpai PK (2018) A hypo-plastic approach for evaluating railway ballast degradation. *Acta Geotech*. <https://doi.org/10.1007/s11440-017-0584-7>
- Du J, Hou K, Liang W, Peng G (2013) Experimental study of compaction characteristics and fractal feature in crushing of coarse-grained soils. *Rock Soil Mech* 34(S1):155–161 (in Chinese)
- Einav I (2007) Breakage mechanics—Part I: theory. *J Mech Phys Solids* 55(6):1274–1297. <https://doi.org/10.1016/j.jmps.2006.11.003>
- Einav I (2007) Breakage mechanics—Part II: modelling granular materials. *J Mech Phys Solids* 55(6):1298–1320. <https://doi.org/10.1016/j.jmps.2006.11.004>
- Einav I (2007) Fracture propagation in brittle granular matter. *Proc R Soc A Math Phys Eng Sci* 463(2087):3021–3035. <https://doi.org/10.1098/rspa.2007.1898>
- Einav I, Valdes JR (2008) On comminution and yield in brittle granular mixtures. *J Mech Phys Solids* 56(6):2136–2148
- Griffith AA (1921) The phenomena of rupture and flow in solids. *Philos Trans R Soc Lond Ser A* 221:163–198
- Group, IC INC (2005) PFC3D Particle flow code in 3 dimensions—command reference. Itasca Consulting Group, Inc, Minneapolis
- Hagerty M, Hite D, Ullrich C, Hagerty D (1993) One-dimensional high-pressure compression of granular media. *J Geotech Eng* 119(1):1–18
- Hardin BO (1985) Crushing of soil particles. *J Geotech Eng* 111(10):1177–1192
- Hertz H (1896) *Miscellaneous papers*. Macmillan, New York
- Houlsby GT, Puzrin AM (2007) *Principles of hyperplasticity: an approach to plasticity theory based on thermodynamic principles*. Springer, Berlin
- Kruyt N, Rothenburg L (1996) Micromechanical definition of the strain tensor for granular materials. *J Appl Mech* 63(3):706–711
- Lade PV, Yamamuro JA, Bopp PA (1996) Significance of particle crushing in granular materials. *J Geotech Eng* 122(4):309–316
- Lee KL, Farhoomand I (1967) Compressibility and crushing of granular soil in anisotropic triaxial compression. *Can Geotech J* 4(1):68–86
- Leung C, Lee F, Yet N (1997) The role of particle breakage in pile creep in sand. *Can Geotech J* 33(6):888–898
- Liu S (2006) Simulating a direct shear box test by DEM. *Can Geotech J* 43(2):155–168
- Liu S, Wang Z, Wang Y, Wang L, Fu Z (2015) A yield function for granular materials based on microstructures. *Eng Comput* 32(4):1006–1024
- Ma G, Zhou W, Ng T-T, Cheng Y-G, Chang X-L (2015) Microscopic modeling of the creep behavior of rockfills with a delayed particle breakage model. *Acta Geotech* 10(4):481–496

36. Ma G, Regueiro RA, Zhou W, Wang Q, Liu JY (2018) Role of particle crushing on particle kinematics and shear banding in granular materials. *Acta Geotech* 13(3):601–618
37. Madadi M, Tsoungui O, Lätzel M, Luding S (2004) On the fabric tensor of polydisperse granular materials in 2D. *Int J Solids Struct* 41(9):2563–2580
38. Marsal RJ (1967) Large-scale testing of rockfill materials. *J Soil Mech Found Div* 93(2):27–43
39. McDowell G, Bolton M (1998) On the micromechanics of crushable aggregates. *Géotechnique* 48(5):667–679
40. McDowell GR, de Bono JP (2013) On the micro mechanics of one-dimensional normal compression. *Géotechnique* 63(11):895
41. McDowell G, Bolton M, Robertson D (1996) The fractal crushing of granular materials. *J Mech Phys Solids* 44(12):2079–2101
42. Mesri G, Vardhanabhuti B (2009) Compression of granular materials. *Can Geotech J* 46(4):369–392
43. Minh N, Cheng Y (2013) A DEM investigation of the effect of particle-size distribution on one-dimensional compression. *Géotechnique* 63(1):44
44. Miura N, Ohara S (1979) Particle-crushing of a decomposed granite soil under shear stresses. *Soils Found* 19(3):1–14
45. Nakata Y, Kato Y, Hyodo M, Hyde AF, Murata H (2001) One-dimensional compression behaviour of uniformly graded sand related to single particle crushing strength. *Soils Found* 41(2):39–51
46. Ouchiyama N, Tanaka T (1981) Porosity of a mass of solid particles having a range of sizes. *Ind Eng Chem Fundam* 20(1):66–71
47. Pestana JM, Whittle A (1995) Compression model for cohesionless soils. *Géotechnique* 45(4):611–632
48. Robertson D (2000) Computer simulations of crushable aggregates. University of Cambridge, Cambridge
49. Roscoe K, Burland JB (1968) On the generalized stress-strain behaviour of wet clay. In: Heyman J, Leckie FA (eds) *Engineering plasticity*. Cambridge University Press, Cambridge, pp 535–609
50. Sammis C, King G, Biegel R (1987) The kinematics of gouge deformation. *Pure Appl Geophys* 125(5):777–812
51. Shaebani MR, Madadi M, Luding S, Wolf DE (2012) Influence of polydispersity on micromechanics of granular materials. *Phys Rev E Stat Nonlinear Soft Matter Phys* 85(1 Pt 1):011301. <https://doi.org/10.1103/PhysRevE.85.011301>
52. Shen C, Liu S, Wang Y (2017) Microscopic interpretation of one-dimensional compressibility of granular materials. *Comput Geotech* 91:161–168
53. Sheng D, Yao Y, Carter JP (2008) A volume–stress model for sands under isotropic and critical stress states. *Can Geotech J* 45(11):1639–1645
54. Tsoungui O, Vallet D, Charmet J-C (1999) Numerical model of crushing of grains inside two-dimensional granular materials. *Powder Technol* 105(1):190–198
55. Tyler SW, Wheatcraft SW (1992) Fractal scaling of soil particle-size distributions: analysis and limitations. *Soil Sci Soc Am J* 56(2):362–369
56. Wood DM, Maeda K (2008) Changing grading of soil: effect on critical states. *Acta Geotech* 3(1):3–14
57. Wu Y, Ma G, Zhou W, Yang L (2016) Optimization of gradation of rockfill materials based on the fractal theory. *Rock Soil Mech* 37(7):1977–1985 (**in Chinese**)
58. Xiao Y, Liu HL, Chen QS, Ma QF, Xiang YZ, Zheng YR (2017) Particle breakage and deformation of carbonate sands with wide range of densities during compression loading process. *Acta Geotech* 12(5):1177–1184
59. Yamamuro JA, Bopp PA, Lade PV (1996) One-dimensional compression of sands at high pressures. *J Geotech Eng* 122(2):147–154
60. Zhang Y, Buscarera G, Einav I (2016) Grain size dependence of yielding in granular soils interpreted using fracture mechanics, breakage mechanics and Weibull statistics. *Géotechnique* 66(2):149–160
61. Zhao C, Yin Z, Misra A, Hicher PY (2018) Thermomechanical formulation for micromechanical elasto-plasticity in granular materials. *Int J Solids Struct*. <https://doi.org/10.1016/j.ijsolstr.2017.12.029>
62. Zhou M, Song E (2016) A random virtual crack DEM model for creep behavior of rockfill based on the subcritical crack propagation theory. *Acta Geotech* 11(4):827–847
63. Ziegler H (2012) *An introduction to thermomechanics*, vol 21. Elsevier, Amsterdam

**Publisher's Note** Springer Nature remains neutral with regard to jurisdictional claims in published maps and institutional affiliations.